Clim Dyn (2011) 36:401–417
DOI 10.1007/s00382-010-0761-y

A statistical–dynamical scheme for reconstructing ocean forcing in the Atlantic. Part II: methodology, validation and application to high-resolution ocean models

Marie Minvielle · Christophe Cassou · Romain Bourdallé-Badie · Laurent Terray · Julien Najac

Received: 6 July 2009 / Accepted: 2 February 2010 / Published online: 6 April 2010

Abstract A novel statistical–dynamical scheme has been developed to reconstruct the sea surface atmospheric variables necessary to force an ocean model. Multiple linear regressions are first built over a so-called learning period and over the entire Atlantic basin from the observed relationship between the surface wind conditions, or predictands, and the anomalous large scale atmospheric circulations, or predictors. The latter are estimated in the extratropics by 500 hPa geopotential height weather regimes and in the tropics by low-level wind classes. The transfer function further combined to an analog step is then used to reconstruct all the surface variables fields over 1958–2002. We show that the proposed hybrid scheme is very skillful in reproducing the mean state, the seasonal cycle and the temporal evolution of all the surface ocean variables at interannual timescale. Deficiencies are found in the level of variance especially in the tropics. It is underestimated for 2-m temperature and humidity as well as for surface radiative fluxes in the interannual frequency band while it is slightly overestimated at higher frequency. Decomposition in empirical orthogonal function (EOF) shows that the spatial and temporal coherence of the forcing fields is however very well captured by the reconstruction method. For dynamical downscaling purposes, reconstructed fields are then interpolated and used to carry out a high-resolution oceanic simulation using the NATL4 (1/4°) model integrated over 1979–2001. This simulation is compared to a reference experiment where the original observed forcing fields are prescribed instead. Mean states between the two experiments are virtually undistinguishable both in terms of surface fluxes and ocean dynamics estimated by the barotropic and the meridional overturning streamfunctions. The 3-dimensional variance of the simulated ocean is well preserved at interannual timescale both for temperature and salinity except in the tropics where it is underestimated. The main modes of interannual variability assessed through EOF are correctly reproduced for sea surface temperature, barotropic streamfunction and mixed layer depth both in terms of spatial structure and temporal evolution. Collectively, our results provide evidence that the statistical–dynamical scheme presented in this two-part study is an efficient and promising tool to infer oceanic changes (in particular those related to the wind-driven circulation) due to modifications in the large-scale atmospheric circulation. As a prerequisite, we have here validated the method for present-day climate; we encourage its use for climate change studies with some adaptations though.

Keywords Weather regimes · Climate variability · Atlantic Ocean · Oceanic forcing variables · Dynamical ocean downscaling

M. Minvielle (✉) · C. Cassou · R. Bourdallé-Badie · L. Terray · J. Najac
CERFACS/CNRS, Climate Modelling and Global Change Team, 42 avenue Gaspard Coriolis, 31057 Toulouse, France
e-mail: minviell@cerfacs.fr

R. Bourdallé-Badie
MERCATOR Parc Technologique du Canal, 8-10 rue Hermès, 31520 Ramonville St Agne, France

1 Introduction

The ocean plays a main role in climate regulation and a correct estimation of the oceanic variability is crucial for climate studies. One important challenge for the next Intergovernmental Panel of Climate Change (IPCC) exercise is to reduce the large uncertainties in both the evaluation of the 3-dimensional oceanic changes that have occurred over the last 50 years or so (e.g. oceanic heat content, wind-driven circulation, meridional overturning circulation—MOC, etc.), and in the projection of these changes for the next century. Coupled General Circulation Models (CGCMs) are traditionally used to understand the climate variability and associated processes. CGCMs are all the more important in a poor observational context because the lack of long-term measurements of the global ocean often leads to conflicting results. Unfortunately, in spite of continuing advances in computational power and scientific understanding, the IPCC-class CGCMs still suffer from important biases (Randall et al. 2007). Some are due to the poor representation of the atmospheric variables at the ocean surface, which are used in air–sea fluxes computation and ensure exchanges between the ocean and the atmosphere. Some are related to the erroneous representation of the interface processes themselves such as feedbacks between sea surface temperature (SST) and turbulent and radiative fluxes (Frankignoul et al. 2004). Note also that the representation of key oceanic processes (e.g. boundary currents, mesoscale eddies, coastal upwellings, etc.) cannot be resolved in IPCC-class CGCMs due to their coarse oceanic resolution (Roberts et al. 2004).

The present two-part study documents a novel statistico-dynamical scheme developed to overcome the systematic biases of global climate models with the ultimate goal to obtain a better estimation of the 3-dimensional ocean mean state and variability for present climate. One of the final perspectives is to assess with more confidence the 3-dimensional changes in response to greenhouse gazes (GHG) increasing concentration over the next century. The proposed method is divided into two distinct steps:

- A statistical step to reconstruct an unbiased forcing dataset for the ocean using the large scale atmospheric circulation from CGCMs. The latter is commonly considered as one of the most reliable outputs from CGCMs by contrast to direct modeled surface atmospheric variables (Christensen et al. 2007). A transfer function is statistically built between the large scale atmospheric circulation (referred as predictors) and the atmospheric surface variables (the predictands) using observations or their best estimates via reanalyzes. This transfer function combined to an analog step is then applied to the modeled atmospheric large scale circulation to reconstruct an atmospheric forcing dataset for the ocean. The statistical step tackles the first source of biases for CGCMs above mentioned, because the mean and the variability of the reconstructed forcing, and consequently of the sea surface ocean to a large extent, are imposed to be close to observation by construction.
- A dynamical step also referred to as dynamical downscaling. The reconstructed atmospheric forcing dataset is used to force an ocean model whose resolution is much higher than in the IPCC-class CGCMs. The higher resolution offers the prospect of credible and coherent representation of smaller-scale processes that are important for local conditions in terms of mean and variability. Dynamical downscaling has been extensively used for the atmosphere. Modeled SSTs from CGCMs are interpolated after bias-correction onto high-resolution atmospheric grids because those correctly represent orography and consequently a large part of precipitation and temperature distribution. By analogy for the ocean, the need for realistic bathymetry appears essential because bottom layer processes control part of the density evolution of the deep outflows (Girton and Sanford 2003) known to be important for the simulation of the oceanic circulation. A better representation of the oceanic deep convection and vertical mixing as well as mesoscale eddies due to higher spatial resolution is also anticipated to be important. Similarly to the atmosphere, forcing fields for the ocean are thus interpolated onto high-resolution ocean grid after biases correction here assessed through the statistical step. The dynamical downscaling step thus tackles the last source of biases of IPCC-class CGCMs above mentioned.

The challenge of the present study is to adapt to oceanic purposes the traditional statistico-dynamical schemes (such as Frey-Buness et al. 1995 or Fuentes and Heimann 2000) usually devoted to regional application over land, and in particular to adapt them to a full-size ocean, here the Atlantic. Attempts for oceanic downscaling have been documented for limited oceanic basins (typically the size of the Baltic Sea, Heyen et al. 1996) but a few papers have tackled a more global perspective. In our case, the crux is to find predictors that capture the coherent variability among *all* the predictands at sea surface (10-m wind, 2-m temperature and humidity, surface radiative fluxes and precipitation) that must be respected in the reconstructed forcing over the *entire* Atlantic Ocean when passed to the high-resolution model. Part I of this study (Cassou et al. 2010) was devoted to this task. We demonstrated that the decomposition in North Atlantic-Europe weather regimes (NAE-WR) in the extratropics and in tropical wind classes (T-WC) representing the alteration of the trades following a so-called weather-typing approach is relevant to derive basin-wide changes of sea surface variables over the entire Atlantic basin from 1958 to 2002. Both the frequency of occurrence of the regimes/classes and their strength assessed through distances to their centroids have been found to be valuable predictors to reconstruct the interannual surface ocean variability as well as trends. In addition, regimes are linked to the alteration of the North Atlantic atmospheric stationary waves considered as the main source of predictability for variability ranging from seasonal to climate change timescale. Recent papers show in particular that the majority of IPCC scenario experiments share a common increase of the stationary wave amplitude associated with the acceleration of the zonal mean wind flow in response to enhanced GHG forcing (e.g. Brandefelt and Körnich 2008). Christensen et al. 2007 in the last IPCC assessment report also mentions that large-scale weather regimes may be considered as one of the most skilful attributes of CGCMs to simulate atmospheric flow patterns. Collectively, the regime entity that can be viewed as a "reading grid" of the large-scale atmospheric circulation, or be interpreted as an efficient spatio-temporal filter of the chaotic atmospheric flow, is a promising candidate for downscaling for both present-day climate and scenarios analyses; NAE-WR and T-WC will thus be our predictors in the following. Before applying the full method to future climate scenarios, its evaluation is necessary for present climate. This study is devoted to this task.

The present paper, or Part II, is organized as follows. The data and the ocean model are presented in Sect. 2. The statistico-dynamical scheme using atmospheric circulation classes as predictors to generate ocean surface variables is detailed in Sect. 3. The statistical step is validated over 1958–2002 and the reconstructed dataset is used to force a high-resolution ocean simulation that is compared to a reference one forced by the original observed dataset. Comparisons between the two simulations are provided in terms of air-sea fluxes and interannual variability for ocean variables in Sects. 4 and 5, respectively. The results are summarized and further discussed in Sect. 6.

2 Data

2.1 The NATL4 ocean model

The high-resolution ocean model used in this study is part of a model hierarchy based on the Nucleus for European Modeling of the Ocean (NEMO) core (Madec 2008) and developed as part of the European model collaboration DRAKKAR (Drakkar group 2007). Its name is NATL4 and corresponds to the regional implementation of NEMO for the Atlantic Ocean at 1/4° resolution on average. The model includes the OPA9 ocean model coupled with the Louvain La Neuve Ice Model version 2 (Fichefet and Morales Maqueda 1999). The horizontal grid is an extraction of the global tripolar ORCA grid at the resolution of 1/4° at the equator (Barnier et al. 2006). The domain covers the Atlantic basin from 20°S to 80°N and includes the Nordic Seas, the Denmark strait and a part of the Western Mediterranean Sea (eastern boundary at 23°E). Buffer zones are defined at all boundaries over 28 grid points with a linear damping time from 3 to 100 days to climatological conditions (Levitus et al. 1998) for the ocean part and to climatological data deduced from a 0.5° global simulation for the ice part. A restoring zone is prescribed in the Gulf of Cadiz bellow 150 m to improve the representation of the Mediterranean outflow. The bathymetry file is deduced from the ETOPO2V2g database (http://www.ngdc.noaa.gov/mgg/fliers/01mgg04.html). On the vertical, there are 50 Z-levels with a resolution of 1 m at the surface, 450 m at the bottom, 26 levels in the upper 250 m and a partial step parameterization is used on the last ocean level (Barnier et al. 2006). The vertical mixing (Blanke and Delecluse, 1993) is based on a turbulent kinetic energy (TKE) scheme. On the horizontal, a filtered free surface (Roullet and Madec 2000), a total variation diminishing (TVD) scheme (Lévy et al. 2001) for the advection of the tracers, an energy and enstrophy conserving scheme (Arakawa and Lamb 1980; Barnier et al. 2006), an isopycnal diffusion for the tracer (300 $m^2\ s^{-1}$) and a biharmonic one for the momentum ($1.5 \times 10^{11}\ m^2\ s^{-2}$) are used. The model starts at rest from climatological conditions for the tracers (Levitus et al. 1998). To avoid artificial drifts due to unbalanced freshwater fluxes, a strong restoring (4 days) to the climatological surface salinity is imposed.

2.2 Large scale circulation and sea surface atmospheric variables

As detailed in Part I, two large-scale atmospheric circulation fields from the European Centre for the Medium-Range Weather Forecasts (ECMWF) ERA40 reanalysis (Uppala et al. 2005) serve as predictors over 1958–2002. NAE-WR are built from daily averaged 500 hPa geopotentiel height (Z500) interpolated on a 2.5° × 2.5° grid. In the tropical band (within 20°S–20°N), T-WC are assessed from the meridional and zonal components of the wind at 1,000 hPa (UV1000). The reader is invited to refer to Part I for further details about the choice for two distinct predictors as a function of the latitudinal domain.

The sea surface atmospheric variables used ultimately after interpolation as forcing fields for NATL4 (predictants for the statistical step) are based on a combination of ECMWF reanalysis products with various satellite datasets. This blended product, hereafter referred to as DFS4 standing for DRAKKAR Forcing Set 4, is fully described in Brodeau et al. (2009) as well as the bulk formulae used for air-sea fluxes computation (Barnier 1998), and the necessary adjustments applied to the raw observed (or estimated) fields to avoid artificial drifts in the ocean simulations. Among those fields,

- 6-h temperature and specific humidity at 2 m, and wind vectors at 10 meters (all on a 1.125° × 1.125° grid) are taken from ERA40 over 1958–2004 and are corrected as detailed by Brodeau et al. (2009).
- daily net shortwave and longwave radiations at the surface are obtained from satellite estimates (ISCCP, Zhang et al. 2004) over 1984–2004. A climatological daily mean deduced from 1984 to 2002 is used for the period 1958–1983. Radiative fields are provided on a T62 gaussian grid (94 × 192 points corresponding to about 1.8 × 1.8° on average)
- monthly total precipitation and snowfall (also on a T62 gaussian grid) are monthly fields from CORE dataset (Large and Yeager 2004) blended with satellite products. Before 1979, we use monthly mean climatology computed over the 1979–2002 period.

3 Statistical algorithm for surface forcing reconstruction

Decomposition of the full Atlantic atmospheric large-scale daily variability into NAE-WR and T-WC wind classes has been found to be discriminatory for oceanic surface variables to be used ultimately as forcings for high-resolution ocean models within a dynamical downscaling framework. In part I, we showed that for a given day, the anomalous air-sea conditions are both linked to the occurrence of the regimes and to the strength and the spatial resemblance of the anomalous large-scale atmospheric circulation with respect to the centroids of the regimes. Based on these results, a multi linear regression model is built in the following to reconstruct surface variables (or predictands) using the distances (or predictors) to all the centroids of the regimes as input for the statistical model. The algorithm presented here is largely inspired from the one described in Boé et al. (2006) and Najac et al. (2008), but adapted to oceanic applications and available observation datasets for surface ocean fields.

3.1 General principle

The methodology can be divided into two separated stages as summarized in Fig. 1. Level 1 is devoted to the construction of the transfer function between predictors and predictands over the so-called learning period. Level 2 corresponds to the use of the model to reconstruct the predictands over the so-called application period. Distinction is made between winter, summer and transition months (see Part I). For the sake of simplicity, let us consider the winter season (DJFM) and only one predictand (hereafter **Y**). Four NAE-WR and four T-WC wind classes are used as predictors for that season.

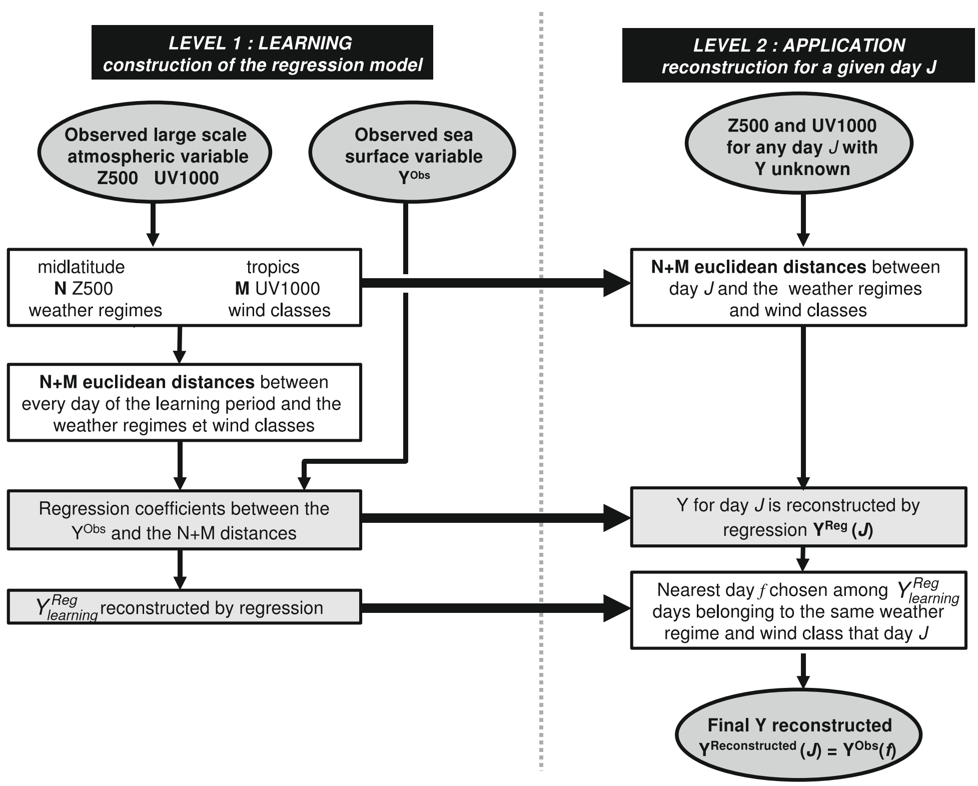

Fig. 1 Flowchart representing the different steps of the statistical reconstruction scheme for 10-m wind

The learning stage (level 1) can be subdivided into three steps. For each winter day over the learning period (*N* days in total), the first step consists in computing the four distances between Z500 anomalies of that day and NAE-WR centroids, and the four distances between UV1000 anomalies and T-WC centroids. As a second step, the $(4 + 4) \times N$ distances are used as input in a multi linear regression model together with observed $\mathbf{Y}$, henceforth $\mathbf{Y}^{\mathrm{Obs}}$, in order to compute the regression coefficients $\boldsymbol{\beta}^k$ following:

$$\mathbf{Y}^{\mathrm{Reg}}_{\mathrm{learning}}(t) = \sum_{k=1}^{k=8} \boldsymbol{\beta}^k \cdot d^k(t) + \boldsymbol{\alpha}$$

where t stands for a given day, k for the number of predictors or regimes, d^k for the Euclidian distance to the kth centroid and $\boldsymbol{\alpha}$ for the residual. In the equation, bold stands for latitude × longitude matrices. Once the regression parameters are set, the regression model is used to reconstruct $\mathbf{Y}$ over the learning period, hereafter $\mathbf{Y}^{\mathrm{Reg}}_{\mathrm{learning}}$. Finally, daily anomalous Z500 and UV1000 maps are classified into NAE-WR and T-WC to form 16 (4×4) groups.

The application stage can be divided into two steps. Let us now consider a given winter day J from observation that does not belong to the learning period. As a first step, $\mathbf{Y}(J)$ is reconstructed using the above-described regression model. This step would be sufficient if the regression model had conserved the variance of the estimated field $\mathbf{Y}^{\mathrm{Reg}}$ which is not the case (von Storch 1999). To overcome this shortcoming, a simple variance inflation technique must be applied as a final step of the reconstruction. Day J is attributed to a given NAE-WR and T-WC based on a minimum distance criterion to centroids. The variance inflation technique consists first in seeking for the analog of $\mathbf{Y}^{\mathrm{Reg}}(J)$ in the pool of $\mathbf{Y}^{\mathrm{Reg}}_{\mathrm{learning}}$ formed by the winter days belonging to the same NAE-WR + T-WC regimes as day J (let f be that particular day and $\mathbf{Y}^{\mathrm{Reg}}_{\mathrm{learning}}(f)$ be the analog). It consists second in "replacing" $\mathbf{Y}^{\mathrm{Reg}}_{\mathrm{learning}}(f)$ by its observed counterpart $\mathbf{Y}^{\mathrm{Obs}}(f)$ so that the variance properties of the reconstructed field are preserved. This final stage of the methodology is often referred to as conditional resampling, "conditional" referring in our case to the restriction in the analog choice based on the belonging to a given NAE-WR + T-WC regimes.

The same procedure is repeated for summer days: ten $\boldsymbol{\beta}^k$ coefficients corresponding to the five JJAS NAE-WR and the five JJAS T-WC are first computed over the learning period (see Part I); $\mathbf{Y}$ is then reconstructed and the choice for analog at the conditional resampling stage is limited to summer regimes. For transition months (AM and ON), we showed that the probability of occurrence for summer and winter regimes is about the same (Part I). Consequently, 18 (8 + 10) distances are used as predictors in the multi linear regression model and there is no restriction for the analog choice at the final reconstruction stage, neither in terms of calendar month nor in terms of belonging to a given regime.

3.2 Application of the reconstruction algorithm to forcing dataset for ocean models

Several surface fields $\mathbf{Y}$ must be reconstructed to ultimately force ocean models: 2 m temperature (T2) and 2 m humidity (Q2), zonal and meridional wind components at 10 m (U10 and V10), longwave and shortwave radiation (LW and SW) and precipitation. In principle, the reconstruction algorithm presented above could be applied to any of these fields $\mathbf{Y}$. In practice, this would lead to inconsistencies among the reconstructed surface variables because the selected day corresponding to the final analog at the conditional resampling stage would be different between those fields. To avoid such an incoherence in the forcing, we decided to apply the reconstruction algorithm *only* to the 10 m wind field (hereafter UV10) treated as our primary predictand among all the surface variables to be reconstructed. Consequently, the selection of the analog day at the end of the reconstruction procedure is given by UV10 and is the same for all the other surface fields. This choice is dictated by the fact that NAE-WR + T-WC are particularly discriminatory for UV10 (see Part I), and secondly because the UV10 intraseasonal variability is very weak compared to the one for the other surface fields.

The more or less dominance of the intraseasonal signal has indeed a strong implication for reconstruction. For UV10, there is no problem in the fact that an analog day for December can been found in March for instance because mean UV10 conditions are virtually the same in December and March; however, it is definitely not the case for the other fields. For instance, temperature is greatly controlled by its seasonal evolution and by the inertia of the ocean. Mean December conditions for T2 largely differ from March conditions because the intraseasonal changes dominate the higher frequency fluctuations (typically daily to weekly). Consequently, the analog day given by the downscaled UV10 and used for T2 by construction cannot be directly considered. Instead of taking the raw T2 of the analog day, its daily anomaly is retained and superimposed to mean daily climatology of the day to be reconstructed (estimated over the learning period). Such a procedure is applied to all surface forcing variables, but UV10 for which we verify that its reconstruction is insensitive to this patch.

3.3 Example

A concrete example is given in the following to better describe all the steps of the reconstruction algorithm as well as the additional adjustments required for radiative fields. Let us pick 18 August 1967 as an example. Ten distances are computed between the NAE Z500 and tropical UV1000 anomalies of that day and the 5 + 5 summer NAE-WR + T-WC that have been determined in a preliminary stage. Those distances are passed to the regression model built over the learning period so that UV10 is reconstructed. The learning period covers all the years over 1958–2002 except the one to be reconstructed, here 1967. We verified that the $\boldsymbol{\beta}^k$ coefficients of the regression model do not depend on the exclusion of the year to be reconstructed, the 45 sets of $\boldsymbol{\beta}^k$ obtained over 1958–2002 being very similar. Based on the minimum distance criterion, 18 August 1967 has been attributed to NAE-WR5 and T-WC2, and the analog for UV10 obtained by regression is then seek in the pool of days formed by the ones where NAE-WR5 and T-WC2 are simultaneously excited over the learning period. Let 1 June 1959 be the analog day.

T2 for 18 August 1967 is reconstructed by taking the T2 daily anomalies of 1 June 1959 and by adding those to the T2 daily climatology of 18 August, in order to preserve T2 seasonal cycle. The same technique is applied for Q2 and could be applied in principle for radiation surface fields SW and LW. Recall however that daily radiative data are only available from 1984. To reconstruct the radiative fields of 18 August 1967 for which the analog day is not available in our example, we therefore look for the subsequent analogs restricted to the NAE-WR5 and T-WC2 pool of days until we found one over 1984–2002 that we can retain. Let 14 July 1997 be that analog. Similarly to T2 and Q2, SW and LW for 18 August 1967 are reconstructed by taking the SW and LW daily anomalies of 14 July 1997 and by adding those to the SW and LW daily climatology of 18 August. Note that this patch is not necessary if the first analog for UV10 belongs to the 1984–2002 period. As to precipitation, because only monthly data are available, we decided to not reconstruct precipitation fluxes in the present study.

4 Validation of the reconstruction algorithm

The statistical method of reconstruction is now validated from two NATL4 simulations forced, respectively, by the original observed DFS4 dataset, or by its reconstruction (hereafter REC). The model is integrated from 1979 to 2001 after a four year spin-up starting from rest. The validation of the reconstructed surface variables is given in the following over 1979–2001 for consistency, despite the regression model at the core of the reconstruction algorithm has been performed over the full 1958–2002 period as detailed in the previous section. NATL4 has not been integrated over 1958–2002 because of computational limitation.

Figure 2 shows the annual zonal means for all the DFS4 surface variables (except for radiative fields) together with their difference with REC. The reconstruction is excellent in terms of mean, and DFS4 and REC are virtually undistinguishable based on t test statistics applied here. This conclusion was expected for T2 and Q2 because the seasonal cycle that dominates the high frequency variability is prescribed by construction in the algorithm. Recall that this is not the case for the zonal and meridional components of wind and we show here that errors in REC are nonetheless very small and not statistically significant in both the tropics and midlatitudes. This indirectly verifies that the resampling at the last stage of the full reconstruction algorithm successfully covers the entire distribution of the anomalous atmospheric circulation assessed through weather regimes/classes (not shown). Figure 3 provides evidence that the reconstruction scheme is also able to capture remarkably well the seasonal cycle of the wind module with the sole assumption that NAE-WR are different between summertime and wintertime. The performance of the method is not function of the domain, the tropics being characterized by a weak seasonal evolution in contrast to midlatitudes.

Differences between DFS4 and REC interannual variability are presented in Fig. 4 for winter and summer boreal seasons taken separately. In boreal winter (Fig. 4a) where

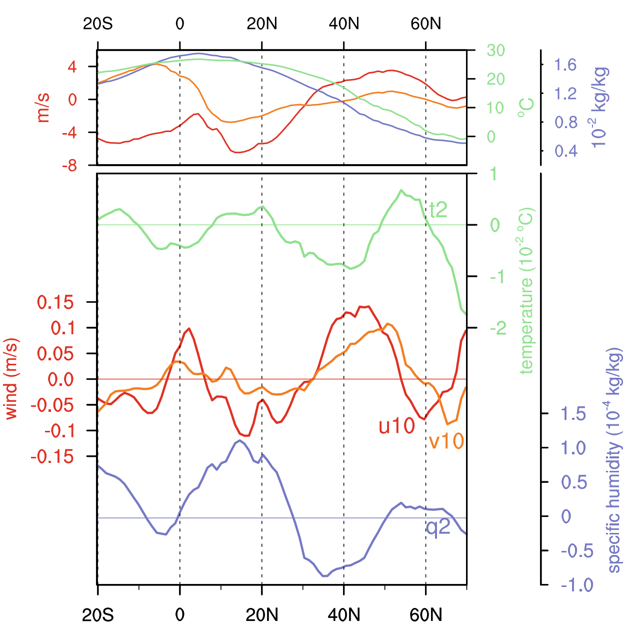

Fig. 2 *Top* Annual zonal mean of 2-m temperature (*green*), specific humidity (*blue*) and 10-m zonal and meridional wind components (*red* and *orange*) for DFS4. *Bottom* Annual zonal mean difference between REC and DFS4. None of the differences are significant based on t statistics at 95%

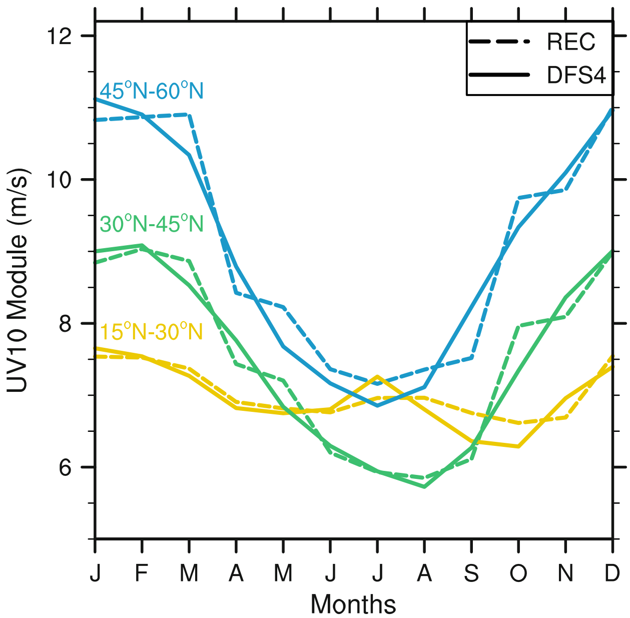

Fig. 3 Mean seasonal cycle of DFS4 and REC 10-m wind module for three latitude bands (15°–30°N, 30°–45°N and 45°–60°N) on the North Atlantic sector. *Solid* (*dashed*) *lines* stands for DFS4 (REC)

maximum variance is found at midlatitudes, the interannual frequency band is well captured in REC for U10 despite a slight underestimation from 40°N northward, and for V10 despite a slight overestimation of the variance from 30°N. About 65% of the interannual variance is captured in REC for the two components of the wind in the northern tropical basin whereas a third of the interannual variance is only reconstructed south of the equator corresponding to summertime there. The interannual variance for T2 and Q2 is underestimated whatever the latitudes with a REC/DFS4 ratio ranging from 0.6 at midlatitudes to 0.15 within the entire tropical band for both thermodynamical variables. In boreal summer (Fig. 4b), interannual variance is considerably weaker for all the variables, except for Q2. The REC surface wind variance is still relatively correct at midlatitudes while it is clearly underestimated in the northern tropical band with value as low as 0.3 for the REC/DFS4 ratio. Note that the shift between the midlatitude and tropical behavior occurs northward in summer compared to winter in agreement with the seasonal latitudinal march of the two dynamics. Note also that the variance loss in the southern tropical basin is less pronounced in JJAS than in DJFM because it is wintertime there. Results are degraded in summer compared to winter for T2 and Q2 especially at midlatitudes where only 20% of the interannual variance are captured by the reconstruction algorithm.

In order to understand the loss of interannual variance in the tropics, let us consider the density spectrum of the tropical wind in DFS4 and REC (Fig. 5). This spectrum is obtained from a daily index of U10 averaged over the 15°–30°N latitude band. As expected, Fig. 5 shows that the variance is clearly underestimated in REC (black line) at low frequencies for periods lower than 10 days and is compensated by an increase at higher frequencies. The persistence of the atmospheric anomalous circulation which is strong in the tropics (high daily autocorrelation values) as opposed to midlatitudes is broken because each

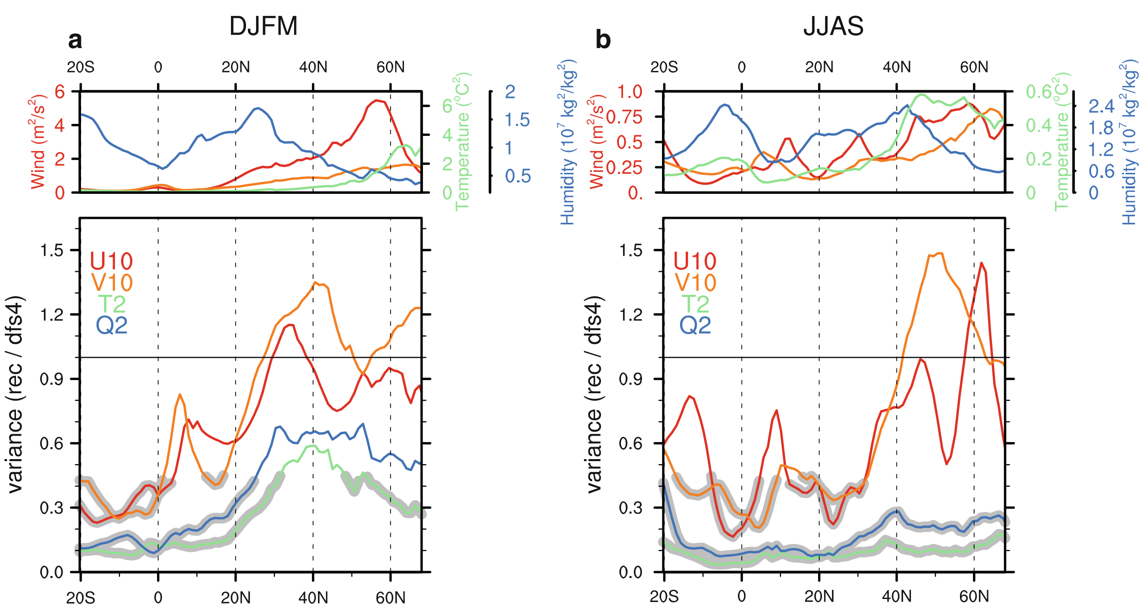

Fig. 4 *Top* Zonal mean of the variance in DJFM (*left*) and JJAS (*right*) for 10-m zonal and meridional wind components (*red* and *orange*, respectively), 2-m temperature (*green*) and specific humidity (*blue*) for DFS4. *Bottom* Ratio between REC and DFS4 zonal mean variance. The *grey* color indicates where the differences of variance between REC and DFS4 are significant (*F* test at 90%)

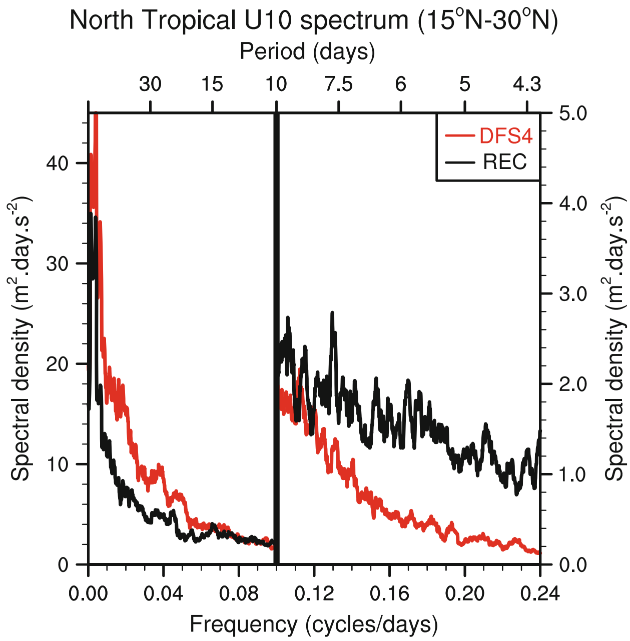

Fig. 5 Spectral density for the daily 10-m zonal wind over the 15°–30°N latitudinal band for DFS4 (*red*) and REC (*black*). The left vertical axis must be considered for frequencies weaker than 0.1 (i.e. 10 days) and the right axis is a zoom for higher frequencies

day is considered as independent at the resampling stage of the algorithm. Artificial variance is thus added by construction in the quasi-daily frequency band at the expense of lower frequencies.

The ability of the method of reconstruction to correctly reconstruct sea surface variables at daily and interannual timescale is finally assessed by means of Taylor diagram (Taylor 2001). Those diagrams are a useful form to estimate the similarity between the two DFS4 and REC datasets in terms of root-mean-square (RMS) and temporal correlation. Only U10 and T2 variables are considered here for three latitudinal bands and two seasons (Fig. 6). As documented above, the interannual variance is well captured for U10 in boreal winter with a ratio near to 1, and is slightly (strongly) underestimated in summer in the extratropics (tropics). The critical loss of power at interannual timescale of the reconstructed variables is confirmed especially for T2 and summertime. The daily variance is very well reproduced with a ratio close to 1 for both variables and both seasons. Regarding the interannual variability, the temporal correlation coefficients show a good agreement in boreal winter between REC and DFS4 (coefficients higher than 0.6). Values are generally a bit stronger for U10 than for T2, and are greater at high latitudes in the 45°–60°N latitude band for both variables. In summer, correlations are smaller, generally below 0.45, except in the Northern basin, with a coefficient equal to 0.5 for T2 and 0.8 for U10. The correlations at daily frequency are small (below 0.4) for U10 for both seasons. Given the large size of the study domain and because of the resampling step of the method, a high daily correlation is not expected: the aim of such a method is more oriented at capturing lower frequency fluctuations typically interannual timescale. Daily correlations are better for T2, but it is important to recall that the T2 daily climatology is prescribed in our reconstruction and artificially provides a good daily temporal correlation. Without imposing the seasonal cycle, the correlation values for T2 daily anomalies are lower than 0.4.

To complete the validation of the reconstruction algorithm, its ability to respect the spatial coherence of the interannual variability of the surface ocean fields is assessed using decomposition in empirical orthogonal function (EOF) of UV10 for winter and summer season and for tropics and extratropics treated separately. In winter and in

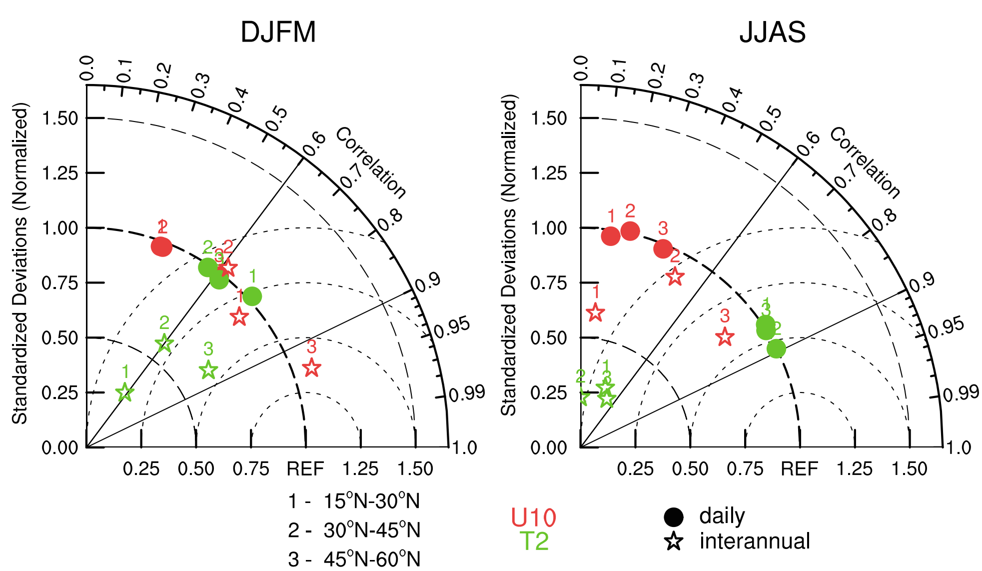

Fig. 6 Taylor diagrams for U10 (*red*) and T2 (*green*) spatially averaged over the 15°–30°N, 30°–45°N and 45°–60°N latitude bands (respectively represented by the numbers *1*, *2*, *3*), for daily fields (*circles*) and seasonal means (*stars*). *Left* (*right*) panel stands for the winter (summer) season

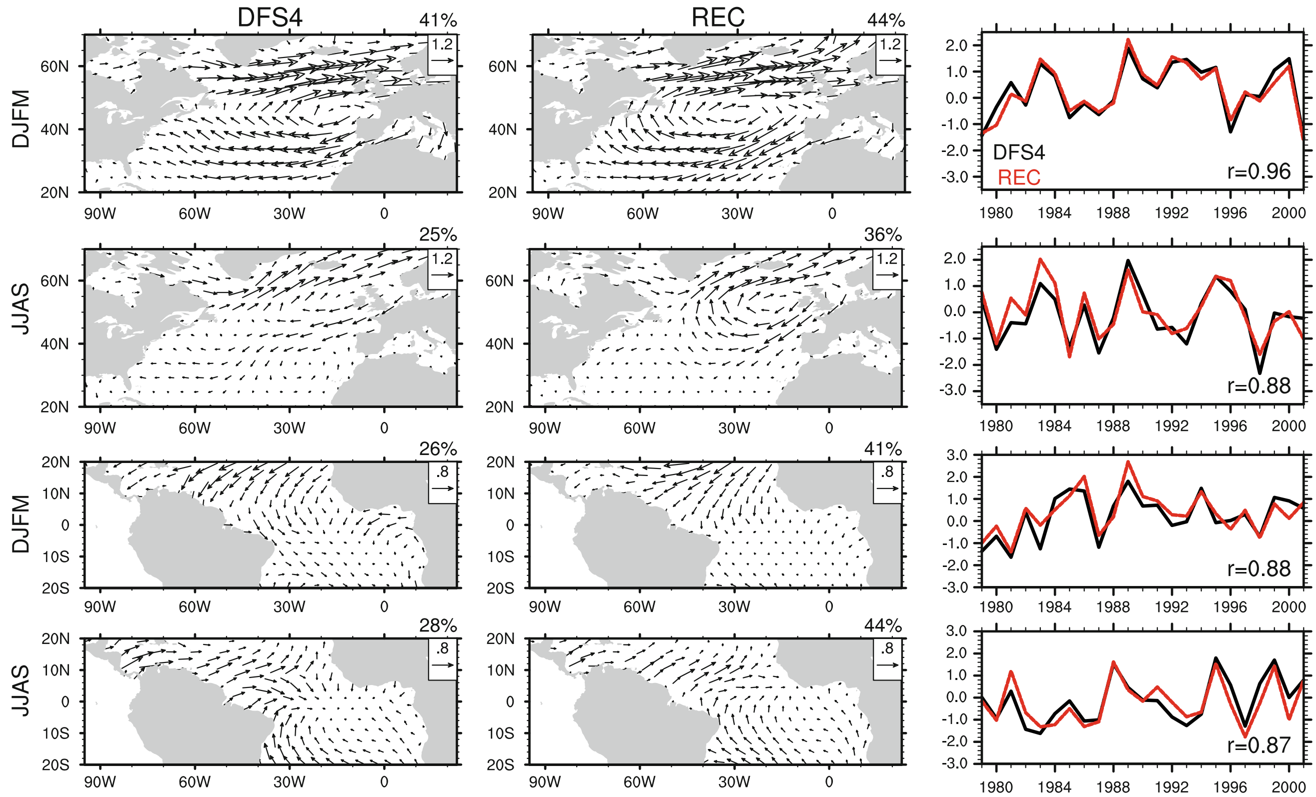

Fig. 7 First EOF of the DJFM and JJAS extratropical and tropical 10-m wind over 1979–2001. *Left and center* DFS4 and REC spatial patterns (m/s) with their respective percentage of explained variance indicated *up right*. *Right* associated normalized principal components for DFS4 (*black*) and REC (*red*). The coefficient correlation between DFS4 and REC principal component is given at the bottom right corner

the extratropics, the dominant mode is characterized in DFS4 by anticyclonic wind anomalies centered off the European coast and related to the NAO (Fig. 7). This structure is very well captured by REC, and despite a slight westward shift of the anomalous core, the spatial correlation between the two maps is equal to 0.85. The correlation of the two time series is equal to 0.96. In summer, the first EOF corresponds to an anticyclonic anomaly centered off the British Islands and is related to the summertime NAO. Spatial and temporal correlations between DFS4 and REC are equal to 0.84 and 0.88, respectively. In the tropical band, the spatial structure of the DJFM leading EOF in DFS4 is characterized by northeasterly wind anomalies restricted to the northern hemisphere and corresponding to reinforced trade winds. The spatial pattern is very similar in REC and spatially correlated at 0.77 while the temporal correlation coefficient between the associated time series is equal to 0.88. The JJAS first EOF corresponds in the northern basin to slackened trade winds and below 10°S to northwestward anomalies leading to equatorial convergence of the winds. The spatial patterns of REC and DFS4 are correlated at 0.77 and their associated principal components at 0.87. Note that the percentage of variance captured by the leading modes is significantly overestimated in all cases in REC, except for the extratropics in winter where DFS4 and REC values are comparable.

5 Application of reconstructed fields to force a high-resolution ocean model

The two NATL4-DFS4 and NATL4-REC high-resolution ocean simulations forced, respectively, by the original observed dataset DFS4 and by its reconstruction REC are now compared in terms of mean and principal modes for interannual variability over 1979–2002. The aim of this work is not to validate the NATL4 model and discuss its skills, but only to validate the impact of the reconstruction method upon the ocean dynamics. Consequently, no comparison with oceanic observations will be provided in the following.

5.1 Mean state and variability of air-sea fluxes

NATL4 computes its own surface turbulent and momentum fluxes using traditional bulk formulae (Brodeau et al. 2009). As expected, based on the results above-described for surface variables, the reconstruction is excellent for the

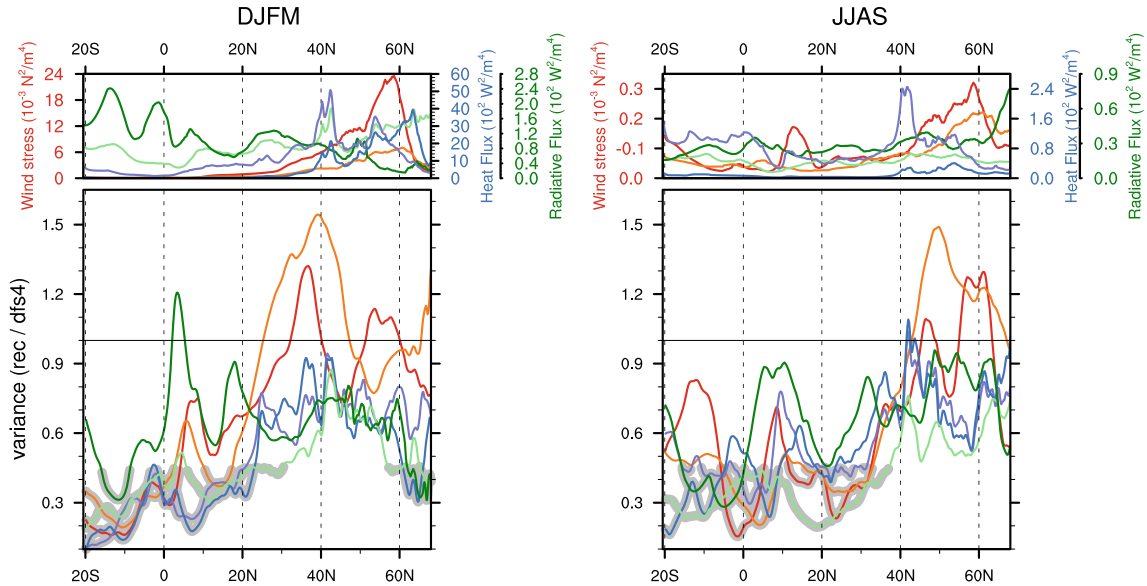

Fig. 8 Same as Fig. 4 but for zonal and meridional wind stress (*red* and *orange*, respectively), shortwave and longwave radiative flux (*dark* and *light green*, respectively), and sensible and latent heat flux (*blue* and *mauve*, respectively) from NATL4-DFS4 and NATL4-REC

surface fluxes in terms of mean (not shown). Differences between NATL4-DFS4 and NATL4-REC interannual variability are presented in Fig. 8 for all the fluxes components for winter and summer boreal seasons treated separately. Most of the biases found for reconstructed surface variables can be tracked down in corresponding surface fluxes with fewer incidences through. Despite T2 and Q2 interannual variance are strongly underestimated, the ones for associated sensible and latent heat fluxes are better captured from 20°N northward where about 75% of the variance is retained in winter instead of 50% for T2. Discrepancies at higher latitude (north of 60°N) are associated with wintertime sea-ice changes in the Labrador Sea. The "recovery" of variance for turbulent fluxes compared to surface variables at midlatitudes holds in summertime provided the seasonal northward migration of the extratropical dynamics. Such a recovery can be explained in part by the correct representation of the reconstructed surface wind (Fig. 2) that directly enters into the turbulent fluxes computation. In the tropics, about two-third of the interannual variance is lost in winter for turbulent fluxes while this bias is clearly diminished in summertime where about 40% of the variance is captured in REC (much better than for T2/Q2). Although reduced, the underestimation of variance for T2 can find its bearing in the longwave component of the radiative fluxes especially in the tropics. The interannual variance of the shortwave radiative flux is relatively well preserved in NATL4-REC with an average level of 70% in both winter and summer seasons in the northern hemisphere. Maximum biases are found over the subtropical highs where low-level clouds that are tightly linked to local ocean temperature control a large part of the interannual shortwave variability. The interannual variance of zonal and meridional wind stress components is very close to the one for U10 and V10, respectively, despite a slight additional boost of variance for the meridional wind stress between 25° and 45°N in winter.

5.2 Validation of oceanic variables

Figure 9a shows the annual zonal means for NATL4-DFS4 SST and Sea Surface salinity (SSS), together with their difference with NATL4-REC. The agreement between the two simulations is excellent for both SST and SSS mean state and there is no statistical difference based on t-test at the 95% level of confidence. Locally, some isolated and very marginal grid points pass the test for some seasons leading on average to slightly cooler (warmer) conditions in NATL4-REC than NATL4-DFS4 between 20°N and 60°N (within the tropical band). The positive bias located north of 60°N is associated with diminished sea-ice cover in the Labrador Sea. For SSS, peaks in difference are produced by very strong eddy activity in the mouth of the main rivers (Amazon river at the equator, Congo, Niger and Mississippi at 8°S, 10°N and 30°N, respectively) and along the gulf stream (around 40°N). Recall that precipitation and river runoff are the same in both experiments suggesting that differences are mostly due to internal ocean dynamics and are not directly linked to the reconstructed forcing. Figure 9b and c show the time evolution of the

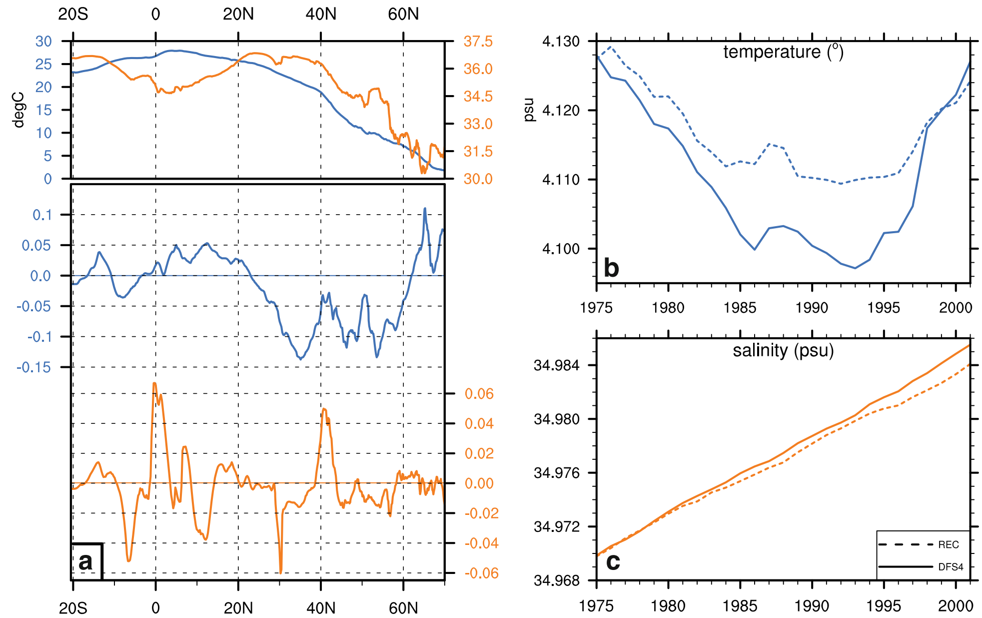

Fig. 9 **a** *Top* Zonal annual mean for SST (*blue*) and SSS (*orange*) in NATL4-DFS4. *Bottom* Difference between NATL4-REC and NATL4-DFS4 SST and SSS. Differences are not significant (*t* test at 95%). Temporal evolution for global 3-dimensional averaged annual temperature (**b**) and salinity (**c**) in NATL4-DFS4 (*solid*) and in NATL4-REC (*dashed*)

3-dimensional temperature and salinity integrated over the entire NATL4 basin. In NATL4-DFS4, a slight cooling (0.04°C in 20 years) occurs until 1993 before a rapid warming. Similar behavior is found in NATL4-REC but trends are less pronounced; interestingly, NATL4-DFS4 and NATL4-REC catch up at the end of the simulation in 2002. The 3-dimensional salinity changes are characterized in both simulations by a spurious trend that clearly overcomes any potential signal coming from the reconstructed forcing. This trend is associated with unbalanced water flux budget shared by both experiments.

NATL4-DFS4 mixed layer depth (MLD) is presented for DJFM average over 1979–2002 as well as its difference with NATL4-REC (Fig. 10a). Both experiments are able to capture the three main ocean convection areas where deep water forms: the Labrador Sea and the Nordic Seas where MLD reaches values as high as 2,200 m in both sites, and the Irminger Sea where convection is a bit shallower. NATL4-REC Labrador and Irminger sites are spatially contracted compared to NATL4-DFS4 and the central core in the Labrador is slightly deepened, but none of these biases are statistically significant based on t-statistics at the 95% level of confidence. The sole significant differences over the entire basin are found in the Nordic Sea where locally the deep convection activity is reduced by 25%. It is difficult to explain and comment the latter disparity

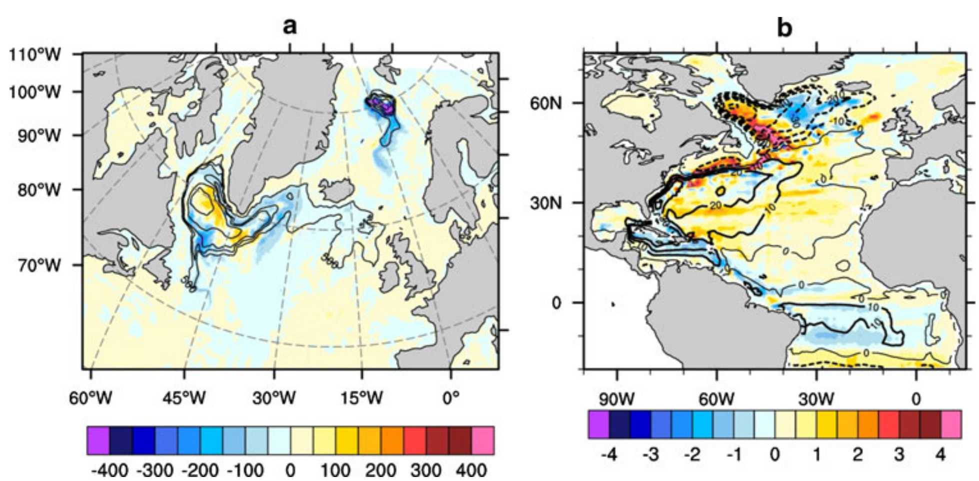

Fig. 10 **a** Contours DJFM mixed layer depth (m) in NATL4-DFS4 (contour interval is 500 m). The maximum value is 2,252 m in the Labrador Sea. *Colors* difference between NATL4-REC and NATL4-DFS4 DJFM mixed layer depth (m). **b** Same as **a** but for annual mean barotropic stream function (contour interval is 10 Sv from −60 to 60). Differences are not significant based on a *t* statistics at the 95% level of confidence

because this convection site is included in the northernmost buffer zone of NATL4.

The large scale ocean mass transport is traditionally split into a horizontal gyre component and a meridional overturning circulation. The latter is equal to 15.5 Sv and 15.1 Sv in NATL4-DFS4 and NATL4-REC, respectively, and differences are not statistically significant. The former is diagnosed via the barotropic streamfunction of the vertically integrated transport and displays a traditional double-gyre circulation of comparable intensity in NATL4-DFS4 (Fig. 10b). The subtropical gyre in NATL4-REC is very close to the one in NATL4-DFS4 even if the tropical circulation feeding the midlatitude branch is slightly underestimated by about 10%. The subpolar gyre appears a bit "distorted" in NATL4-REC with stronger recirculation in the Irminger Sea while the western boundary Labrador Current appears to be less intense. Maximum differences are found off Newfoundland but are barely significant because this area is characterized by very strong mesoscale variability. Based on additional experiments (not shown), we suspect that a large part of the NATL4-DFS4 and NATL4-REC discrepancies are not directly linked to the reconstructed forcing but rather explained by internal model dynamics. In any case, the mean horizontal circulation structure is very well reproduced in NATL4-REC.

The interannual variance in NATL4-DFS4 and in NATL4-REC is examined for temperature and salinity from annual zonal means as a function of depth (Fig. 11). Two plumes of maximum variance are found in the extratropics. The midlatitude core around 40°N corresponds to strong vertical mixing along the mean position of the North Atlantic storm track, and to the presence of mesoscale eddies along the Gulf Stream path. The northernmost core is associated with strong interannual variability of deep water formation where convection occurs in the Labrador and Irminger Seas. The 3-dimensional interannual variance is very well captured in NATL4-REC in the extratropics and Fig. 11 confirms that the reduced variance in the upper-ocean due to underestimated variance in the reconstructed forcing does not significantly penetrate at depth. In the tropics, the entire wind-driven subtropical cells seem however to be more impacted by slackened forcings. Significant underestimation of variance by about 75% extends down to 300–400 m with respect to the equator and is particularly pronounced in the southern hemisphere both in temperature and salinity. Such a tropical bias is clearly related to the lost variance in surface tropical wind and surface temperature in NATL4-REC. Note that the reconstruction algorithm has been developed to optimally reproduce the Northern Hemisphere

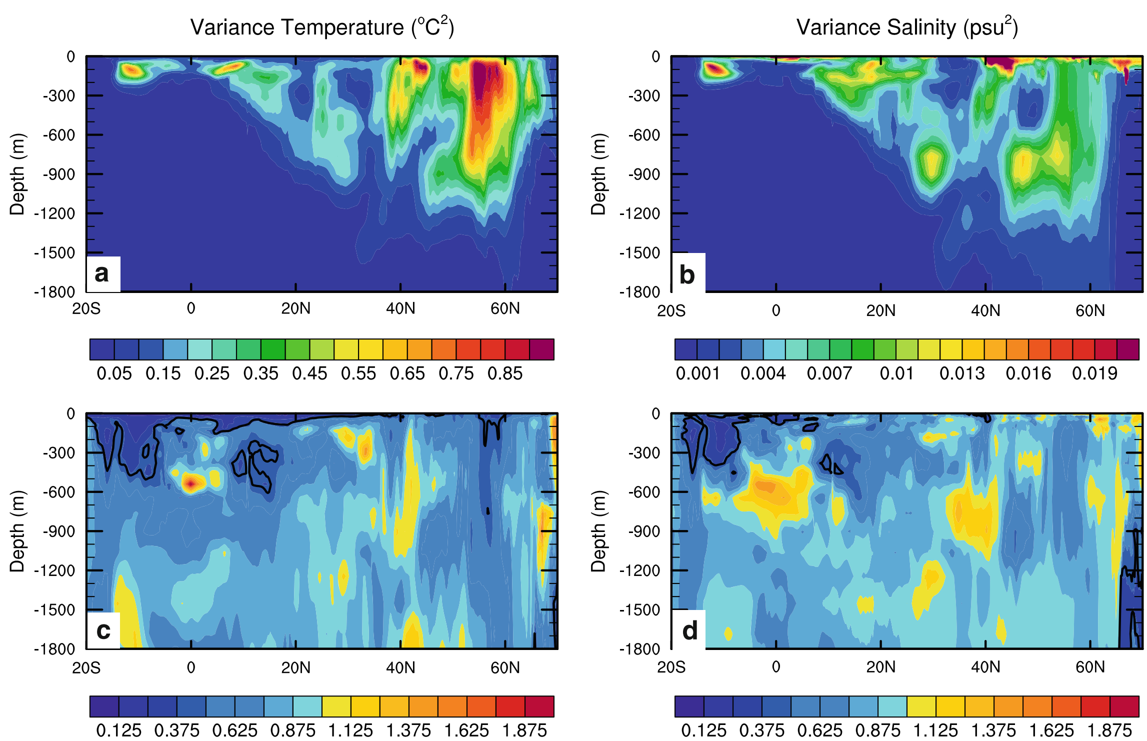

Fig. 11 Variance of annual zonal mean temperature (**a**,°C²) and salinity (**b**, psu²) in NATL4-DFS4. Ratio of annual zonal mean variance of temperature (**c**) and salinity (**d**) between NATL4-REC and NATL4-DFS4. *Black contours* indicate the 90% level of significance based on *F* statistics

fluctuations and therefore can not pretend to fully represent the variability south of the Equator. Lastly, significant diminished variance for salinity is found at depth in the high latitude. The interpretation of this core is nevertheless subject to caution because it is located in the northernmost buffer zone of NATL4.

In the subsequent analyses, we use EOF to identify the spatial structure and the temporal behavior of the dominant modes of interannual variability in the North Atlantic. A traditional cosine weighting as a function of latitude is applied to annual averaged field and we limit our comparison to the two leading EOFs in NATL4-DFS4 and NATL4-REC. For SST, those accounts for about 50% of the total variance in both experiments and are displayed in Fig. 12, together with their normalized principal components (PC). EOF1 is characterized in NATL4-DFS4 by a global warming of the North Atlantic with maximum loading at the southern tip of Greenland (Fig. 12a). Isolated cooling occurs at the northern edge of the Gulf Stream as well as in the Norwegian Sea, but those areas stay marginal. This mode could be interpreted either as a trend or as a shift around 1994–1995 between two mean SST states associated with the two phases of the Atlantic Multidecadal Oscillation (Knight et al., 2005). The dominant mode of NATL4-DFS4 is well captured in NATL4-REC although the explained variance and SST anomalies of the reconstructed pattern are slightly weaker. The spatial correlation between NATL4-REC and NATL4-DFS4 maps is equal to 0.81 and their PCs are correlated at 0.88. EOF2 is characterized in NATL4-DFS4 by a tripole structure (Fig. 12b): subtropical and high latitudes SST, especially in the Labrador Sea, are cold while midlatitudes SST, especially along the Gulf Stream and over the extreme Northeastern basin, are concurrently warmer. This mode can be interpreted as the surface ocean response to NAO forcings (e.g. Cayan 1992): its PC is correlated at 0.65 with the annual NAO index estimated from ERA40 sea level pressure. NATL4-REC EOF2 bears a strong resemblance to NATL4-DFS4 both in terms of spatial structure (maps correlated at 0.74) and temporal variability (PC correlated at 0.91). Note that EOF2 explained variance is slightly greater in NATL4-REC than in NATL4-DFS4, and that SST anomalies are slightly weaker consistently with the underestimated variance of the reconstructed fields at low frequency as reported in Sect. 4.

The two leading EOF for annual barotropic streamfunction (Fig. 13) are also very similar between NATL4-DFS4 and NATL4-REC. EOF1 is characterized by a spin-up of the subpolar gyre concomitant with a strengthening of the Gulf Stream up to 1996–1997. Spatial correlation between NATL4-DFS4 and NATL4-REC EOF1 maps is equal to 0.88 and reaches 0.97 for their time series; their explained variance is comparable. EOF2 mostly captures the meridional displacement of the Gulf Stream and the variability in the inter gyre circulation. Time series suggest a strong correlation between EOF2 and the NAO

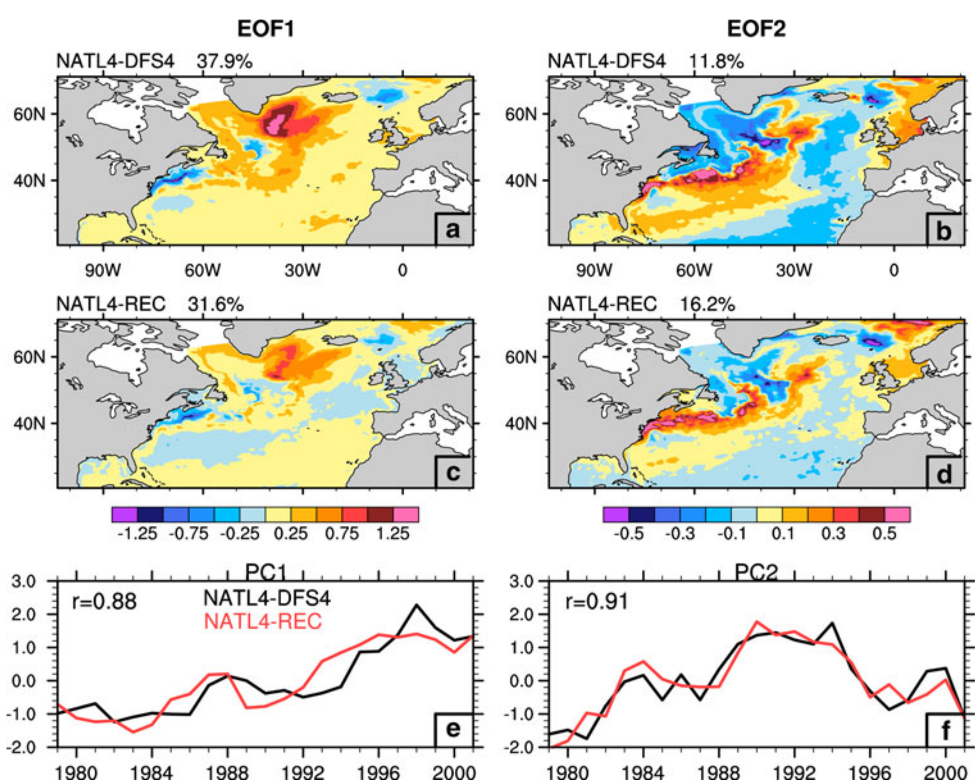

Fig. 12 First (*left column*) and second (*right column*) EOF of annual SST (°C) for (**a**, **b**) NATL4-DFS4 and (**c**, **d**) NATL4-REC over 1979–2001. The percentage of explained variance for each pattern is indicated at the *upper left corner*. Associated normalized principal components for NATL4-DFS4 (*black*) and NATL4-REC (*red*). The correlation between the PCs is given at the *top left corner*

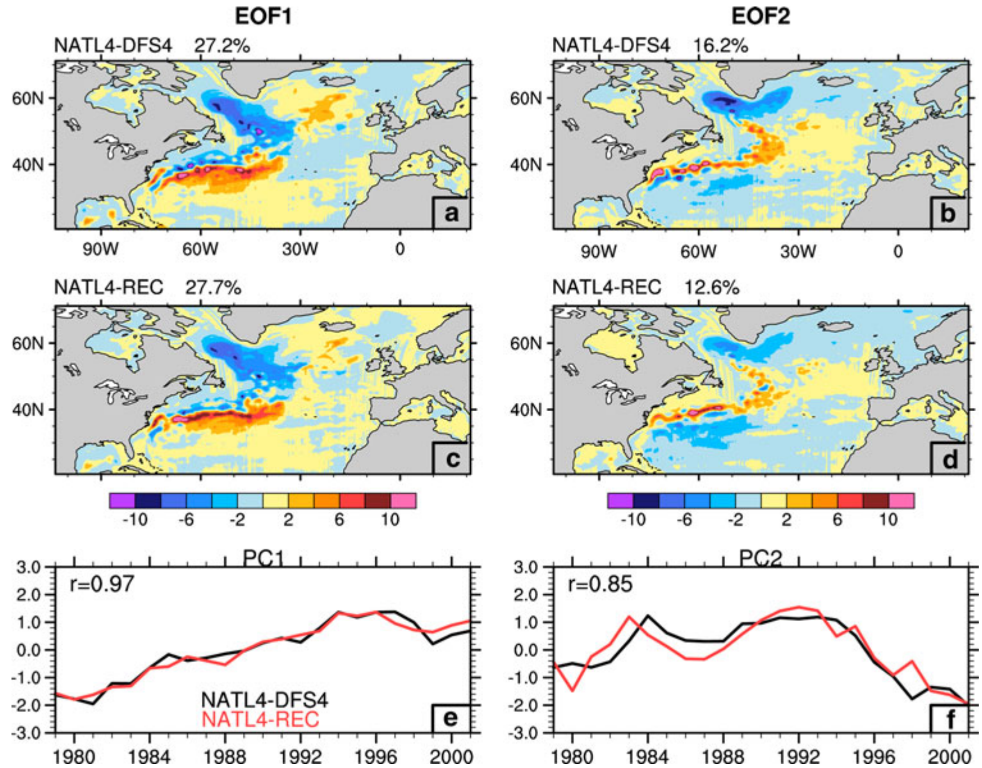

Fig. 13 Same as Fig. 12 but for the annual barotropic stream function (Sv)

index, positive NAO being associated with the northward expansion of the subtropical gyre (Curry and McCartney 2001) and the intensification/contraction of the northernmost part of the subpolar gyre. Those fluctuations can be tracked down in the MLD variability as featured by the leading EOF of winter MLD (Fig. 14) for NATL4-DFS4 and NATL4-REC. Enhanced convection in the Labrador and Irminger Seas occurs in the mid-1980s and early 1990s while it is diminished in the Nordic Seas, before a clear reversal from 1996 onwards. EOF1 captures more than half of the total variance in both NATL4-DFS4 and NATL4-REC. The spatial correlation between the two experiments EOF is equal to 0.93 and the temporal correlation between their PC reaches 0.65.

The ability of the method of reconstruction to reproduce the dominant modes of variability at interannual timescale in the tropics is now evaluated. The leading EOF of NATL4-DFS4 annual mean tropical SST is characterized by a basin-wide signal with maximum loading along the equator and the African coast; it represents about half of the explained variance (Fig. 15a). This mode can be interpreted as the tropical signature of the AMO as suggested by the very strong correlation (0.86) between its PC and the annual mean AMO index (http://www.cdc.noaa.gov/Correlation/amon.us.long.data). This mode is not capture by the reconstruction method. EOF1 in NATL4-REC is characterized by a dipole between the northern and southern tropical basin with respect to the mean position of the Inter Tropical Convergence Zone. The latter is often referred to as the interhemispheric mode that dominates the tropical climate fluctuations at interannual timescale (e.g. Ruiz-Barradas et al. 2000). This mode corresponds to EOF2 in NATL4-DFS4 as shown in Fig. 15b; the spatial correlation between NATL4-DFS4 EOF2 and NATL-REC EOF1 is equal to 0.8 and their respective PCs are correlated at 0.63. Figure 15 provides evidence that the reconstruction scheme is able to capture a large part of the interannual variability but is deficient in reproducing the very low frequency oceanic signals such as the AMO. Such a failure can be attributed to the weak coupling between the daily atmospheric circulation upon which the reconstruction algorithm is based, and the tropical imprint of the AMO.

6 Conclusion and perspectives

A novel statistical method has been developed to reconstruct atmospheric surface variables over the Atlantic basin to be ultimately used as forcing for high-resolution ocean models. In a companion paper (Part I), we have characterized the links between the large scale atmospheric circulation structures and the surface ocean conditions. We have demonstrated that the decomposition of the daily atmospheric circulation into weather regimes over the North Atlantic-Europe region, and into wind classes over the Tropical Atlantic, is relevant to derive basin-wide

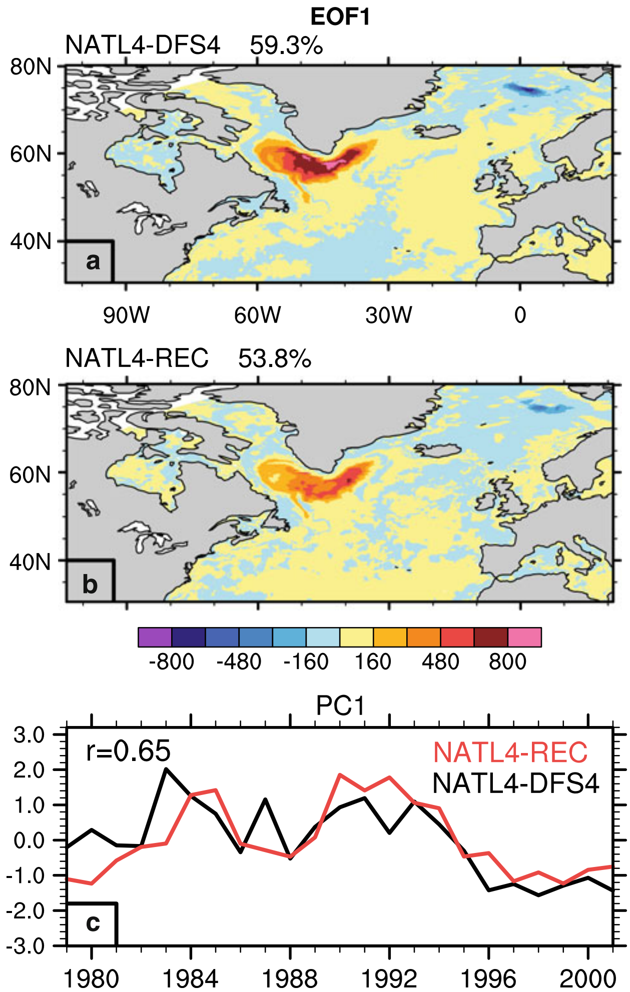

Fig. 14 Same as Fig. 12 but for EOF1 only and for the DJFM mixed layer depth (m)

changes of surface atmospheric variables. A statistical relationship based on multiple linear regressions is thus built between the distances to the extratropical + tropical regimes/classes used as predictors, and the observed surface wind conditions over a so-called learning period. The transfer function combined to a conditional resampling step based on analogue is then used to reconstruct all the surface ocean fields over 1958–2002. Winter and summer seasons are treated separately. Emphasis is laid on the necessary modifications which have been introduced in this study compared to traditional reconstruction schemes described in literature. Indeed, we have to deal here with a domain of large size combining tropical and extratropical dynamics, and with the fact that several variables must be reconstructed at once to conserve the physical coherence. Accordingly, we have chosen to treat the surface wind field as the primary variable to be reconstructed and to derive the others parameters (T2, Q2, radiation) from the latter.

The performance of the statistical method is validated in two steps. First, we compare the distribution properties and the variability of the reconstructed surface variables REC with the reference dataset DFS4. We conclude that:

- the reconstruction scheme is able to perfectly reproduce the mean state of the surface variables both in the tropics and at midlatitudes,
- the daily variance of the forcing fields is very well captured,
- the seasonal cycle is quasi perfectly respected for the wind field without any assumptions. Recall that the latter is prescribed for the other variables,
- the interannual fluctuations of the wind are correctly reconstructed. Analyses based on EOF decomposition provide evidence that the reconstruction algorithm is skilful in retaining the spatial and temporal coherence of the forcing fields at interannual timescale. Deficiencies are found in the level of variance that is largely underestimated in the interannual frequency band especially in the tropics for 2-m temperature and humidity as well as for radiative fluxes. Such a bias is more pronounced in summertime. This is the principal weakness of the proposed scheme. Our study should be interpreted as a first attempt and poor skill in the tropics clearly deserves more investigation and probably some additional adaptations (choice of the predictors in terms of variables and techniques, etc.).

As a second step of validation, we have carried out two numerical experiments using the NATL4 high-resolution ocean model where we prescribe either REC or DFS4 as atmospheric forcings. Mean states between the twin experiments are virtually undistinguishable both in terms of surface fluxes and ocean dynamics estimated by the barotropic and the meridional overturning streamfunctions. The 3-dimensional temperature and salinity and the main positions of the deep convection sites are well reproduced. The 3-dimensional variance of the simulated ocean is well preserved at interannual timescale both for temperature and salinity except in the tropics; note that the biases in terms of fluxes are attenuated compared to those for the raw atmospheric forcing variables. The main extratropical modes of variability assessed through EOF are very similar in NATL4-REC and NATL4-DFS4 both in terms of spatial structure and temporal evolution for SST, barotropic streamfunction and mixed layer depth showing the ability of the method of reconstruction to capture a large part of the interannual variability, especially in the extratropics. However, as expected, the underestimation of the low frequency variance for the forcing fields can be tracked down in the ocean simulation within the tropical band and is a clear limit of our study. Note also that NATL4-REC does not capture the leading EOF mode of tropical SST representing the AMO. The length of the simulation could be too short to firmly believe in this conclusion, but

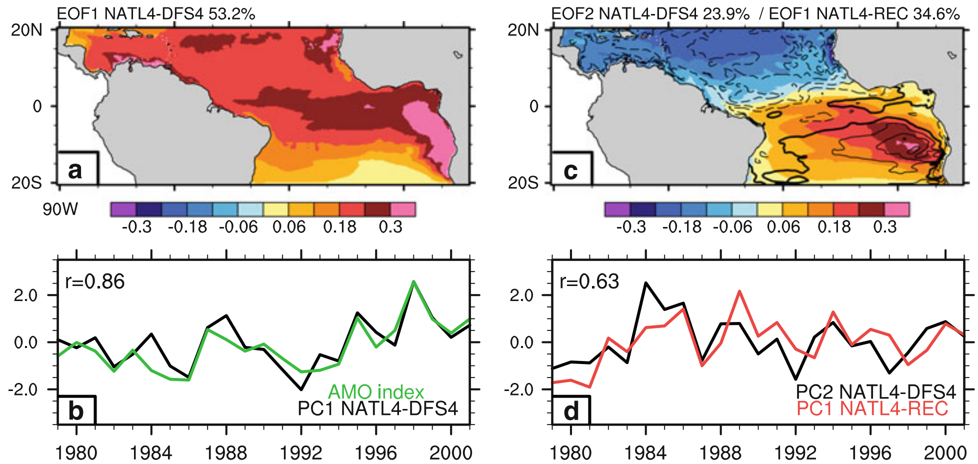

Fig. 15 **a** Spatial pattern of the EOF1 NATL4-DFS4 annual mean SST (°C) and **b** normalized principal component (*black line*). The standardized AMO index (*green line*) is superimposed and the coefficient correlation between the two time series is indicated at the *top left corner*. **c** Spatial pattern of EOF2 NATL4-DFS4 (*color*) and EOF1 NATL4-REC (*contour*) annual mean SST (°C). **d** Normalized PC2 of NATL4-DFS4 (*black*) and PC1 of NATL4-REC (*red*). The correlation between the two time series is given at the *top left corner*

preliminary results using the ½ degree resolution for NEMO (ORCA05) and integrated over 1958–2002 suggest that the model ocean is still unable to represent the AMO. Recall that the reconstruction scheme is able to reproduce the main tendencies of all the atmospheric forcings but for T2 (see part I). This would suggest that the AMO is weakly coupled to the daily atmospheric circulation and would have a different origin (e.g. surface signature of thermohaline variability, etc.). In addition, the direct radiative forcing from increased GHG concentration appears to be a good candidate to explain T2 trends. By construction, this factor that is not related to atmospheric dynamics is impossible to be captured in the present framework.

The results validated here for present climate and from observational estimates are very promising for ocean downscaling applications of future climate scenarios. As mentioned in the Introduction, reconstructing atmospheric datasets provide an alternative to overcome the biases in surface fluxes generally simulated in CGCMs used traditionally in IPCC reports. Following the framework adopted here, large-scale predictors are taken from CGCMs while the forcing fields for the ocean are reconstructed based on the transfer function presented here. In a preliminary study, we have verified using the Météo-France CNRM-CM3 model that the statistical scheme is indeed very skilful in representing the twentieth century variability. Some non-trivial adaptations of the scheme are necessary though for the twenty-first century scenario because the reconstruction is built on the stationarity hypothesis that changes between the predictants and the predictors are the same, and that an analogue can be found in the present climate at the conditional resampling stage of the algorithm. This is clearly not the case for T2 as already documented in Yiou et al. (2007) over land even for the 2000s. A large part of the future T2 increase is not due to indirect atmospheric circulation changes but to the direct contribution of radiative forcing from increased GHGs concentrations. This additional factor must be added in the reconstruction scheme. There are several ways to estimate it. As a first step, we use the trend of the global average of T2 computed from all the IPCC AR4 models and add this trend to the reconstructed value, similarly to what has been proposed in Boé et al. (2006). Preliminary results using CNRM-CM3 outputs suggest that the 3-dimensional ocean changes are sensitive to this additional term. In our case, it even appears to be the main actor in the projected slowdown of the MOC at the end of the twenty-first century. More investigations are needed though to draw firmer conclusions and will be presented in a forthcoming paper. Another limit of such a reconstruction scheme for future climate is associated with the "forced" experimental protocol because it is strongly suspected that some mechanisms at work in climate change greatly result from ocean–atmosphere coupling that is not represented in high-resolution ocean model only.

Another interesting perspective could be to apply the method of reconstruction to outputs from monthly-to-seasonal prediction systems. Daily atmospheric fields from operational climate forecasts could be reconstructed to obtain an unbiased forcing dataset to be applied in very high-resolution model used in ocean operational forecasts. The statistical–dynamical scheme presented here appears as an efficient and promising tool to infer small scale oceanic changes (in particular those related to the wind-driven circulation) due to modifications in the large-scale atmospheric circulation. This could have direct applications for coastal studies.

Acknowledgments The authors are very grateful to Julien Boé for very simulating discussions. We thank Eric Maisonnave for his assistance. Laurent Brodeau and Jean-Marc Molines are gratefully acknowledged for the use of the DFS4 forcing dataset developed at MEOM-LEGI, Grenoble. The figures were produced with the NCL software developed at NCAR. The simulations were performed at the computing center of Météo-France, Toulouse. This work was supported by CERFACS, CNRS, Mercator-Ocean via the DESAGO project and by the European Community via the sixth framework ENSEMBLES project under Contract GOCE-CT-2003-505539.

References

Arakawa A, Lamb PJ (1980) A potential enstrophy and energy conserving scheme for the shallow water equations. Mon Wea Rev 109:18–36

Barnier B (1998) Ocean modeling and parameterization, chapter forcing the ocean. Kluwer, The Netherlands, pp 45–80

Barnier B et al (2006) Impact of partial steps and momentum advection schemes in a global ocean circulation model at eddy permitting resolution. Ocean Dyn. doi:10.1007/s10236-006-0082-1

Blanke B, Delecluse P (1993) Variability of the tropical Atlantic ocean simulated by a general circulation model with two different mixed layer physics. J Phys Oceanogr 23:1363–1388

Boé J, Terray L, Habets F, Martin E (2006) A simple statistical–dynamical downscaling scheme based on weather types and conditional resampling. J Geophys Res 111:D23106. doi:10.1029/2005JD006889

Brandefelt J, Körnich H (2008) Northern Hemisphere stationary waves in future climate projections. J Clim 21:6341–6353

Brodeau L, Barnier B, Treguier AM, Penduff T, Gulev SK (2009) An ERA40 based atmospheric forcing for global oceanic circulation models. Ocean Model 31(3–4):88–104. doi:10.1016/j.ocemod.2009.10.005

Cassou C, Minvielle M, Terray L and Perigaud C (2010) A statistical-dynamical scheme for reconstructing ocean forcing in the Atlantic. Part I: Weather regimes as predictors for surface ocean variables. Clim Dyn. doi:10.1007/s00382-010-0781-7

Cayan DR (1992) Latent and sensible heat flux anomalies over the northern oceans: driving the sea surface temperature. J Phys Oceanogr 22:859–881

Christensen JH (2007) Regional climate projections. In: Salomon S et al (eds) Climate change 2007: the physical science basis. Cambridge University Press, Cambridge, pp 847–940

Curry RG, McCartney MS (2001) Ocean gyre circulation changes associated with the North Atlantic Oscillation. J Phys Oceanogr 31:3374–3400

Drakkar Group (2007) Eddy-permitting ocean circulation windcasts of past decades, CLIVAR Exchanges 12. International CLIVAR project office, Southampton, UK, pp 8–10

Fichefet T, Morales Maqueda MA (1999) Modelling the influence of snow accumulation and snow ice formation on the seasonal cycle of the Antarctic sea-ice cover. Clim Dyn 15:251–268

Frankignoul C, Kestenare E, Botzet M, Carril AF, Drange H, Pardaens A, Terray L, Sutton R (2004) An intercomparison between the surface heat flux feedback in five coupled models, COADS and the NCEP reanalysis. Clim Dyn 22:373–388

Frey-Buness F, Heimann D, Sausen R (1995) A statistical–dynamical downscaling procedure for global climate simulations. Theor Appl Climatol 50:117–131

Fuentes U, Heimann D (2000) An improved statistical–dynamical downscaling scheme and its application to the Alpine precipitation climatology. Theor Appl Climatol 65:119–135

Girton JB, Sanford TB (2003) Descent and modification of the overflow plume in the Denmark Strait. J Phys Oceanogr 33:1351–1364

Heyen H, Zorita E, von Storch H (1996) Statistical downscaling of monthly mean North Atlantic air-pressure to sea level anomalies in the Baltic Sea. Tellus A 48:312–323

Knight JR, Allan RJ, Folland CK, Vellinga M, Mann ME (2005) A signature of persistent natural thermohaline circulation. Geophys Res Lett 32:L20708. doi:10.1029/2005GL024233

Large WG, Yeager SG (2004) Diurnal to decadal global forcing for ocean and sea-ice models: the data sets and flux climatologies. NCAR Technical Note NCAR/TN-460+STR

Levitus S, Boyer TP, Conkright ME, OBrien T, Antonov J, Stephens C, Stathoplos L, Johnson D, Gelfield R (1998) World Ocean Database 1998, No. 18 in NOAA Atlas NESDIS, US Department of Commerce

Lévy M, Estublier A, Madec G (2001) Choice of an advection scheme for biogeochemical models. Geophys Res Lett 28:3725–3728

Madec G (2008) NEMO reference manual, ocean dynamics component: NEMO-OPA. Preliminary version. Note du Pole de modélisation, Institut Pierre-Simon Laplace (IPSL), France, No 27 ISSN No 1288–1619

Najac J, Boé J, Terray L (2008) A multi-model ensemble approach for assessment of climate change impact on surface winds in France. Clim Dyn. doi:10.1007/s00382-008-0440-4

Randall DA (2007) Climate models and their evaluation. In: Salomon S et al (eds) Climate change 2007: the physical science basis. Cambridge University Press, Cambridge, pp 589–662

Roberts MJ, Banks H, Gedney N, Gregory J, Hill R, Mullerworth S, Pardaens A, Rickard G, Thorpe R, Wood R (2004) Impact of an Eddy-permitting ocean resolution on control and climate change simulations with a global coupled GCM. J Clim 17:3–20

Roullet G, Madec G (2000) Salt conservation, free surface and varying volume: a new formulation for ocean GCMs. J Geophys Res Oceans Res 105:23927–23942

Ruiz-Barradas A, Carton JA, Nigam S (2000) Structure of interannual-to-decadal climate variability in the tropical Atlantic sector. J Clim 13:3285–3297

Taylor KE (2001) Summarizing multiple aspects of model performance in single diagram. J Geophys Res 106:D7. doi:10.1029/2000JA002008

Uppala SM et al (2005) The ERA40 re-analysis. Q J R Meteorol Soc 131:2961–3012

Von Storch H (1999) On the use of "inflation" in statistical downscaling. J Clim 12:3505–3506

Yiou P, Vautard R, Naveau P, Cassou C (2007) Inconsistency between atmospheric dynamics and temperatures during the exceptional 2006/2007 fall/winter and recent warming in Europe. Geophys Res Lett 34:L21808. doi:10.1029/2007GL031981

Zhang YC, Rossow WB, Lacis AA, Oinas V, Mishchenko MI (2004) Calculation of radiative fluxes from the surface to top of atmosphere based on ISCCP and other global data sets: refinements of the radiative transfer model and the input data. J Geophys Res 109:D19105. doi:10.1029/2003JD004457